be much greater than that of CO_2, the data are nevertheless consistent with a relatively short lifetime for CO and with dilution of the radioactive CO by CO produced by combustion. If the radioactive CO is uniformly distributed in the atmosphere like radioactive CO_2, then we can derive the content of radioactive CO in the atmosphere. If we take the average specific activity of the South Buffalo samples to be 12.3 disintegrations min^{-1} g^{-1} and the decay constant of ^{14}C to be 9.6×10^{12} disintegrations min^{-1} g^{-1}, the ratio of radioactive CO to stable CO in the samples is 1.3×10^{-12}. If we use 0.3 ppm for the atmospheric concentration of radioactive CO for these samples, the global concentration of radioactive CO is then 4×10^{-13} ppm. The mass of the atmosphere is 5×10^{21} g, which gives 1 kg for the mass of ^{14}C in the atmosphere as CO. If we assume that the removal mechanism for CO is first-order with respect to CO and that the radioactive CO in the atmosphere is in a steady state, the effective rate constant for the removal of radioactive CO is then 3×10^{-7} sec^{-1} (the rate of formation of ^{14}C is 1.3×10^{19} atom sec^{-1}) (*9*). The lifetime of CO in the atmosphere is then 3×10^6 seconds or 0.1 year.

This value is probably too low, because radioactive CO, which is principally produced in the stratosphere, may be converted to radioactive CO_2 in significant amounts before it mixes into the troposphere. The same process would have a much smaller effect on the CO produced by combustion on the earth's surface because in that case the total removal would be limited by mass transport of the larger quantity of CO from the troposphere to the stratosphere. A likely process for the conversion to CO to CO_2 in the stratosphere is the reaction (*2*)

$$CO + OH \rightarrow CO_2 + H$$

The same reaction could be an effective mechanism for the removal of CO, in the troposphere, but Bates and Witherspoon did not consider it likely. If we assume that CO is in a steady state at a concentration of 0.1 ppm in the atmosphere, we can calculate the concentration of OH required to maintain the steady state from

$$[OH] = P/k[CO]$$

where P is the rate of CO production (3.5×10^4 molecule cm^{-3} sec^{-1}) derived from Robinson and Robbins's estimate (*6*) of 2.1×10^{14} g $year^{-1}$ and an atmospheric volume of 4.1×10^{24} cm^3, and k is the second-order rate constant, 2×10^{-13} cm^3 $molecule^{-1}$ sec^{-1} (*13*). The concentration of OH required to maintain CO at a concentration of 0.1 ppm is then 7×10^4 molecule cm^{-3}. This is not unreasonably high but could only be realized by a regenerative chain mechanism for OH because of the large amount of CO involved. The following steps coupled with the previous reaction is one possibility:

$$H + O_2 + M \rightarrow HO_2 + M$$

and

$$H + HO_2 \rightarrow 2OH$$

Thus consideration of the data on radioactive carbon provides additional support for a short lifetime for CO in the atmosphere. This should help to dispel further the concern that CO is accumulating in the atmosphere and represents a longtime hazard to human health. A quantitative assessment of the CO removal processes remains to be worked out, but the action of certain microorganisms and of photochemical processes offer reasonable, possible explanations.

BERNARD WEINSTOCK
Ford Motor Company,
Scientific Research Staff,
Dearborn, Michigan 48121

References and Notes

1. M. V. Migeotte, *Phys. Rev.* **75**, 1108 (1949).
2. D. R. Bates and A. E. Witherspoon, *Mon. Notic. Roy. Astron. Soc.* **112**, 101 (1952).
3. M. V. Migeotte, private communication to D. R. Bates.
4. M. Stephenson, *Bacterial Metabolism* (Longmans, Green, London, ed. 3, 1949).
5. G. W. Jones and G. S. Scott, *Ind. Eng. Chem.* **31**, 775 (1939).
6. E. Robinson and R. C. Robbins, *Sources, Abundance, and Fate of Gaseous Atmospheric Pollutants* (Stanford Research Institute project PR-6755, prepared for the American Petroleum Institute, New York, 1967).
7. W. F. Libby, *Radiocarbon Dating* (Univ. of Chicago Press, Chicago, ed. 2, 1955).
8. ———, *ibid.*, p. 15.
9. ———, *ibid.*, p. 7.
10. F. Johnson, *ibid.*, chap. 7.
11. M. Pandow, C. MacKay, R. Wolfgang, *J. Inorg. Nucl. Chem.* **14**, 153 (1960).
12. C. MacKay, M. Pandow, R. Wolfgang, *J. Geophys. Res.* **68**, 3929 (1963).
13. G. Dixon-Lewis, W. E. Wilson, A. A. Westenberg, *J. Chem. Phys.* **44**, 2877 (1966).

11 June 1969; revised 23 July 1969

Spectrographic Detection of Topographic Features on Mars

Abstract. *Observations of the martian carbon dioxide band at 1.05 microns made with a three-channel multislit spectrophotometer indicate gross height variations in the vicinity of Syrtis Major and surrounding desert regions. Syrtis Major appears to be very high with essentially no detectable carbon dioxide above it. The data appear to confirm local trends and, in magnitude at least, the large variations of height found in earlier radar observations. A one-to-one correlation of height with albedo is not evident in the results. Elevated areas are found in both desert and dark regions. In several regions dark areas are associated with relatively steep slopes.*

The question of the relative altitudes of the dark and bright areas on Mars has been hotly debated in recent years. Traditionally the dark areas are considered to be lowlands. This view is based mainly on the idea that they would be warmer and therefore more likely to support the life forms that were thought responsible for the remarkable regenerative property of the dark areas (*1*). This supposition received some support when the dark areas were in fact generally found to be some 8°K warmer than the bright regions. Others (*2*) have shown that the temperature variations have little to do with height differences. They assert that temperature is more closely connected with the local surface albedo. They propose that the regenerative property is a purely mechanical, wind-driven phenomenon and have concluded that the dark areas are probably higher than the bright deserts. Some quantitative evidence for this view has been provided by early radar data (*3*) as well as by certain observations of cloud phenomena (*4*). More recently, radar mapping (*5*) along a narrow belt at 23°N latitude has indicated very large height variations of some 12 km. However, there does not appear to be any obvious correlation between the radar height contour and albedo changes.

We have devised a three-channel, multislit photometer which, together with the 13.4-m spectrometer of the McMath Solar Telescope of Kitt Peak National Observatory, is capable of de-

tecting altitude variation of less than 1 km over lateral scales of 850 km (at closest approach). The instrument will be described in detail elsewhere, with only a brief description here. The 8.2-mm diameter image of Mars was stabilized electronically on the entrance aperture of the spectrometer (*6*) which is formed by an image slicer (1 by 1 mm). This defines the relevant lateral scale on the planet. At the exit aperture there are 16 slits that are scribed on a mirror. Each has an effective width of 0.09 Å. The slits pass light centered on the J0-J28 lines and the head region of the R-branch of the (123) CO_2 band at 1.05 μ into two cooled detectors (ITT FW118 S-1 photomultipliers). Lines of low excitation are measured by channel 1, and lines of high excitation by channel 2. Channel 3 accepts light in the continuum reflected from the front surface of the mirror in the region between the lines. A fourth detector, sampling light from an emission line source, has the double purpose of calibrating the instrument in wavelength and guarding against wavelength drifts. Another line from the same source provides for calibration of the relative efficiency of the individual slits. The basic photometric calibration is done by observing the moon and an intermediate laboratory continuum source.

If S_1, S_2, and S_3 are the detected signals in channels 1, 2, and 3, then the theory of the instrument, as used by us, shows that

$$R \equiv 1 - \gamma_1(S_1/S_3) - \gamma_2(S_2/S_3) = \Sigma b_J(W_J/\delta_J)/\Sigma b_J \quad (1)$$

where γ_1 and γ_2 are factors obtained from the photometric calibration; b_J, the individual slit efficiency factors; W_J, the equivalent width of the line with rotational quantum number J; and δ_J, the exit slit width for the line. In practice we do not measure S_i ($i = 1, 2, 3$) directly but obtain S_1/S_3 and S_2/S_3 by integrating the pulses in channels 1 and 2 until S_3 reaches a preset count.

If the lines in the band are weak, that is, if they are linearly proportional to the amount of absorber in the line of sight, and if the b_J are not too different from one another, then R is essentially independent of the temperature and depends only on the amount of absorber in the line of sight. We have shown from data obtained at both this and the 1967 opposition (*6*) that the above conditions are effectively satisfied, with the exception that it is better to use $W_J \sim (\eta N)^{0.72}$ rather than a linear law (η is the air mass factor; N, the vertical column density of gas). The power law takes care of the fact that the lines are just reaching saturation at their centers under the conditions present in the martian atmosphere. The insertion of this expression for W_J into Eq. 1 introduces a slight temperature dependence back into R, but we neglect this. Thus

$$R = \text{constant } (\eta N)^k \quad (2)$$

if we simplify the situation further by assuming the presence of an isothermal atmosphere above the planet's surface

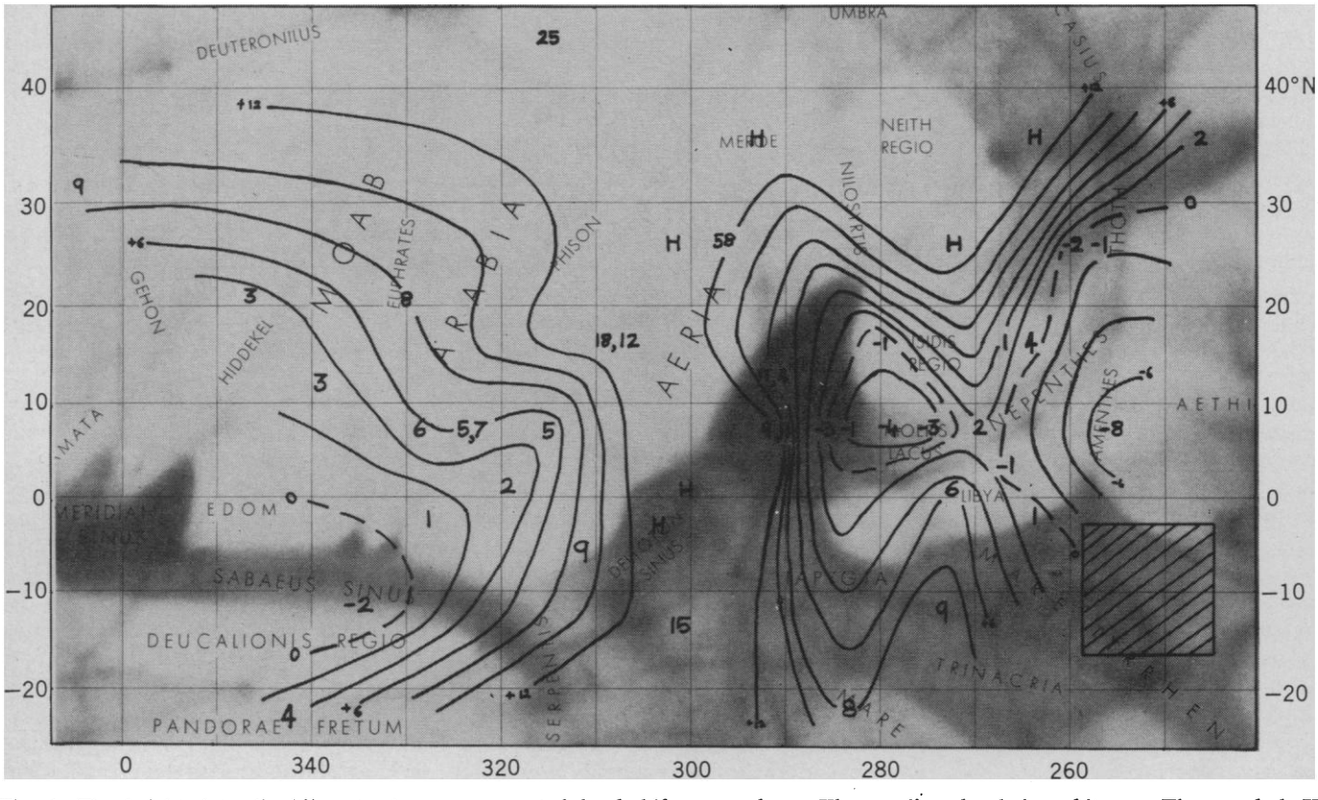

Fig. 1. The height data (in kilometers) are represented by boldface numbers. The median level is arbitrary. The symbol **H** indicates that, effectively, no CO_2 was detected by the instrument; **H** may, therefore, be interpreted as "high." Drawing the rough contours at 2-km differences in height was accomplished by interpolating linearly between adjacent data points. It should be recognized that this process is relatively subjective and can introduce spurious features. Points marked **H** and those with altitudes greater than 15 km were assumed to be at 15 km above the median level when drawing the contours. A small but significant correction to counteract the effects of differential refraction is not included in this preliminary analysis. The approximate spatial resolution element is indicated by the rectangle (marked with hatching) in the bottom right-hand corner of the figure. The map on which the contours are drawn was produced for NASA by the U.S. Air Force.

(k is the slope of the curve of growth). Then the height $\bar{z}$ of the surface above a suitably defined mean level is introduced into the expression

$$R = \text{constant } (\eta)^k \exp(-k\bar{z}/H) \quad (3)$$

Here H is the scale height in the atmosphere, which we have taken as 10 km. Our 1967 data indicated that $k = 0.72$ for lines in this band, and we have taken $R = 0.12$ at $\eta = 2$ to define a mean level for the surface. This choice of zero level is, at the present stage of reduction, quite arbitrary and we are not able to assign a specific value of the partial pressure of CO_2 to it; the most we can say is that our previous value of 5 millibars seems to be roughly consistent.

On the evening of 1 June/2 June (Mountain Standard Time) we were fortunate enough to have moderately fair skies and excellent seeing, which allowed us to obtain data on the regions surrounding and including the very dark feature Syrtis Major. (After 4½ years of observing Mars with the solar telescope this was the first time that we could easily recognize features on the planet.) Figure 1 shows the distribution of heights which was obtained from the data by means of Eq. 3. The numbers are given in kilometers. By linearly interpolating between the data points we constructed a contour map of the region: lines are drawn at 2-km intervals. It is important to note that much of the detail that appears in the contours is due to the numerical interpolation and is probably unreal (*7*). What should be significant is the general trend and direction of the slopes. The spatial resolution element is also shown on the diagram. The following preliminary conclusions can be drawn: (i) Syrtis Major is part of a high ridge that has relatively steep slopes. According to the one measurement that was precisely centered on the feature there was essentially no detectable CO_2 above it. (ii) Highlands are not restricted to the dark areas. This is in accordance with the radar data of Counselman *et al.* (*5*). (iii) The vertical scale of height variations is of the order of 10 km, which is also in agreement with the radar data. (iv) In several regions dark areas coincide with strong slopes (*8*).

MICHAEL J. S. BELTON
DONALD M. HUNTEN
Planetary Sciences Division,
Kitt Peak National Observatory,
Tucson, Arizona 85717

References and Notes

1. For a review of early ideas on the nature of the dark areas, consult G. deVaucouleurs, *Physics of the Planet Mars* (Faber, London, 1953).
2. D. G. Rea, *Nature* **201**, 1014 (1964); C. Sagan and J. B. Pollack, *J. Geophys. Res.* **73**, 1373 (1968).
3. C. Sagan, J. B. Pollack, R. M. Goldstein, *Astron. J.* **72**, 20 (1967).
4. R. A. Wells, *Nature* **207**, 735 (1965).
5. C. C. Counselman, G. H. Pettengill, I. I. Shapiro, *Trans. Amer. Geophys. Union* **49**, 217 (1968); I. I. Shapiro, *Sci. Amer.* **219**, 28 (July 1968).
6. M. J. S. Belton, A. L. Broadfoot, D. M. Hunten, *J. Geophys. Res.* **73**, 4795 (1968).
7. The presence of very high regions on the map, simply marked **H** because of the absence of a detectable amount of CO_2 over the area, raises the question of the accuracy of the data. The uncertainty in height is given by $\delta z = (-H/k)\,\delta R/R$, where δR is the uncertainty in the ratio R. For heights close to the zero level $\delta R/R$ is approximately equal to 0.1, giving an uncertainty of about 1.5 km. At greater elevations, that is, as R tends to zero, δz increases exponentially with height. Thus the highest regions are quite uncertain. The opposite is true for regions whose altitude is less than the zero level. Errors due to temperature variations are much more difficult to analyze and a discussion of them will be omitted here. They are not expected to be significant, however.
8. Contribution No. 461 from the Kitt Peak National Observatory, operated by the Association of Universities for Research in Astronomy, Inc., under contract with the National Science Foundation. We thank A. L. Broadfoot, I. R. Gordon, and P. Carlson for important contributions.

16 June 1969

Massive Internal Fracture of an Amorphous Polyester

Abstract. When amorphous polyethylene terephthalate is subjected to a tensile load of 2 to 4 × 10⁸ dynes per square centimeter within the approximate temperature range 40° to 70°C, an unusual optical effect occurs. The transparent polymer film is suddenly transformed into a brilliantly reflecting strip with the luster of silver. Extensive formation of voids accounts for the unorthodox behavior.

An unusual optical effect can be observed when amorphous polyethylene terephthalate film is dead-loaded in tension. This report describes the effect, its possible nature, and the stress-temperature conditions under which it occurs.

Polyethylene terephthalate (PET) is usually available in semicrystalline form, and it is in that state that it finds use as textile fiber and as film for electrical and other applications. When cooled rapidly below the melting point (265°C), PET can be fabricated into relatively rigid, transparent film or fiber that diffracts x-rays in the manner characteristic of amorphous liquids. Amorphous PET fibers can be stretched homogeneously at constant extension rate until a constriction (or "neck") forms that becomes stable when the cross section of the fiber drops to about 30 percent of the original area (*1*). Once formed, the neck travels along the specimen and consumes it in a process known as cold-drawing (*2*) (Fig. 1).

We deformed rectangular strips of amorphous PET film (*3*) in the temperature region 40° to 70°C by dead-loading rather than by stretching at constant elongation rate. When the stress imposed was sufficiently low, the specimen responded in elastic manner at first by elongating rapidly, but thereafter extended very slowly and apparently homogeneously in the manner characteristic of rigid viscoelastic bodies in creep. Such behavior was observed in the region of the stress-temperature plane which is marked "homogeneous creep" in Fig. 2. When the stress exceeded a certain threshold (Fig. 2), cold-drawing, rather than homogeneous creep, occurred after a waiting period which ranged from 1 second to about 15 minutes. Further increase of the load led to a sudden and remarkably fast elongation of the specimen to several times its original length and its simultaneous conversion from a transparent to a brilliantly reflecting strip with the luster of silver (Fig. 1). This rapid optical transformation occurred under stress-temperature conditions which are labeled "internal fracture" (Fig. 2). At even higher stresses, the specimens became lustrous, but then almost immediately failed ("compound fracture," Fig. 2). Additional increase of the stress invariably led to rapid

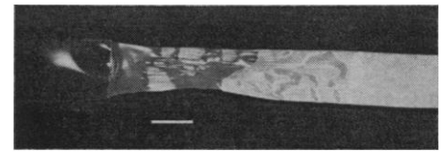

Fig. 1. A strip of amorphous polyethylene terephthalate subjected to a dead tensile load of 2.55×10^8 dynes/cm² (about 3700 psi) at 63.5°C. (Extreme left) Transparent undrawn specimen; (middle) cold-drawn translucent section containing patches of opaque, lustrous material; (right) highly reflecting, silvery material. Scale, 1 cm.